ACS APPLIED MATERIALS & INTERFACES

www.acsami.org

Research Article

Solution-Gated Ultrathin Channel Indium Tin Oxide-Based Field-Effect Transistor Fabricated by a One-Step Procedure that Enables High-Performance Ion Sensing and Biosensing

Toshiya Sakata,* Shoichi Nishitani, Akiko Saito, and Yuta Fukasawa

Cite This: https://doi.org/10.1021/acsami.1c05830

Read Online

ACCESS | Metrics & More | Article Recommendations | Supporting Information

ABSTRACT: In this paper, we propose a one-step procedure for fabricating a solution-gated ultrathin channel indium tin oxide (ITO)-based field-effect transistor (FET) biosensor, thus providing an "all-by-ITO" technology. A thin-film sheet was placed on both ends of a metal shadow mask, which were contacted with a glass substrate. That is, the bottom of the metal shadow mask corresponding to the channel was slightly raised from the substrate, resulting in the creeping of some particles into the gap during sputtering. Owing to this modified metal shadow mask, a thin ITO channel (<30−40 nm) and thick ITO source/drain electrodes (ca. 100 nm) were simultaneously fabricated during the one-step sputtering. The thickness of ITO films was critical for them to be semiconductive, depending on the maximum depletion width (~30−40 nm for the ITO channel), similarly to 2D materials. The ultrathin ITO channel worked as an ion-sensitive membrane as well owing to the intrinsic oxidated surface directly contacting with an electrolyte solution. The solution-gated 20-nm-thick channel ITO-based FET, with a steep subthreshold slope (SS) of 55 mV/dec (pH 7.41) attributable to the electric double-layer capacitance at the electrolyte solution/channel interface and the absence of interfacial traps among electrodes formed in one step, demonstrated an ideal pH responsivity (~56 mV/pH), resulting in the real-time monitoring of cellular respiration and the long-term stability of electrical properties for 1 month. Moreover, the chemical modification of the ITO channel surface is expected to contribute to biomolecular recognition with ultrahigh sensitivity owing to the remarkably steep SS, which provided the exponential pH sensitivity in the subthreshold regime. Our new device produced in this one-step manner has a great future potential in bioelectronics.

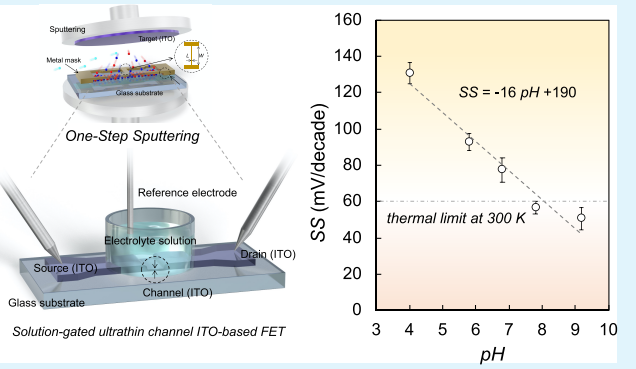

KEYWORDS: *solution-gated field-effect transistor (FET), one-step procedure, ultrathin channel, indium tin oxide (ITO), 2D material*

1. INTRODUCTION

Solution-gated field-effect transistors (FETs) have attracted attention owing to their applicability to biological sensing. The first solution-gated FETs were based on a silicon-based semiconductor with a thin gate insulator that was contacted with an electrolyte solution, where the gate potential was controlled through a reference electrode.[1] Oxide and nitride membranes used as the gate insulator and the passivation layer, respectively, can effectively detect a change in pH on the basis of the equilibrium reaction between hydrogen ions and hydroxy groups at the surface.[2,3] Afterward, various ion-sensitive membranes and biomimetic receptors with enzymes, antibodies, and single-stranded DNAs were coated on the gate electrode to specifically and selectively detect target ions and biomolecules with charges,[4−11] and cellular activities were monitored on the basis of the change in ionic behaviors at the cell/gate interface in real time.[12−15] This is because the detection principle of FET biosensors is basically derived from the potentiometric measurement of the changes in ionic and biomolecular charges or membrane capacitances at the electrolyte solution/gate electrode interface. Moreover, various semiconductive materials have been widely utilized as the channel of FETs for biosensing devices, such as one-dimensional [1D (e.g., nanotubes and nanowires)] and two-dimensional [2D (e.g., graphene, diamond, and MoS_2)] materials.[16−20] On the other hand, 2D channel transport properties were investigated in terms of channel thickness from a monolayer to bulk (multilayer) in a vacuum prober with a cryogenic system.[21−23] When the channel thickness of 2D materials was smaller than the maximum depletion width,

Received: March 30, 2021
Accepted: July 26, 2021

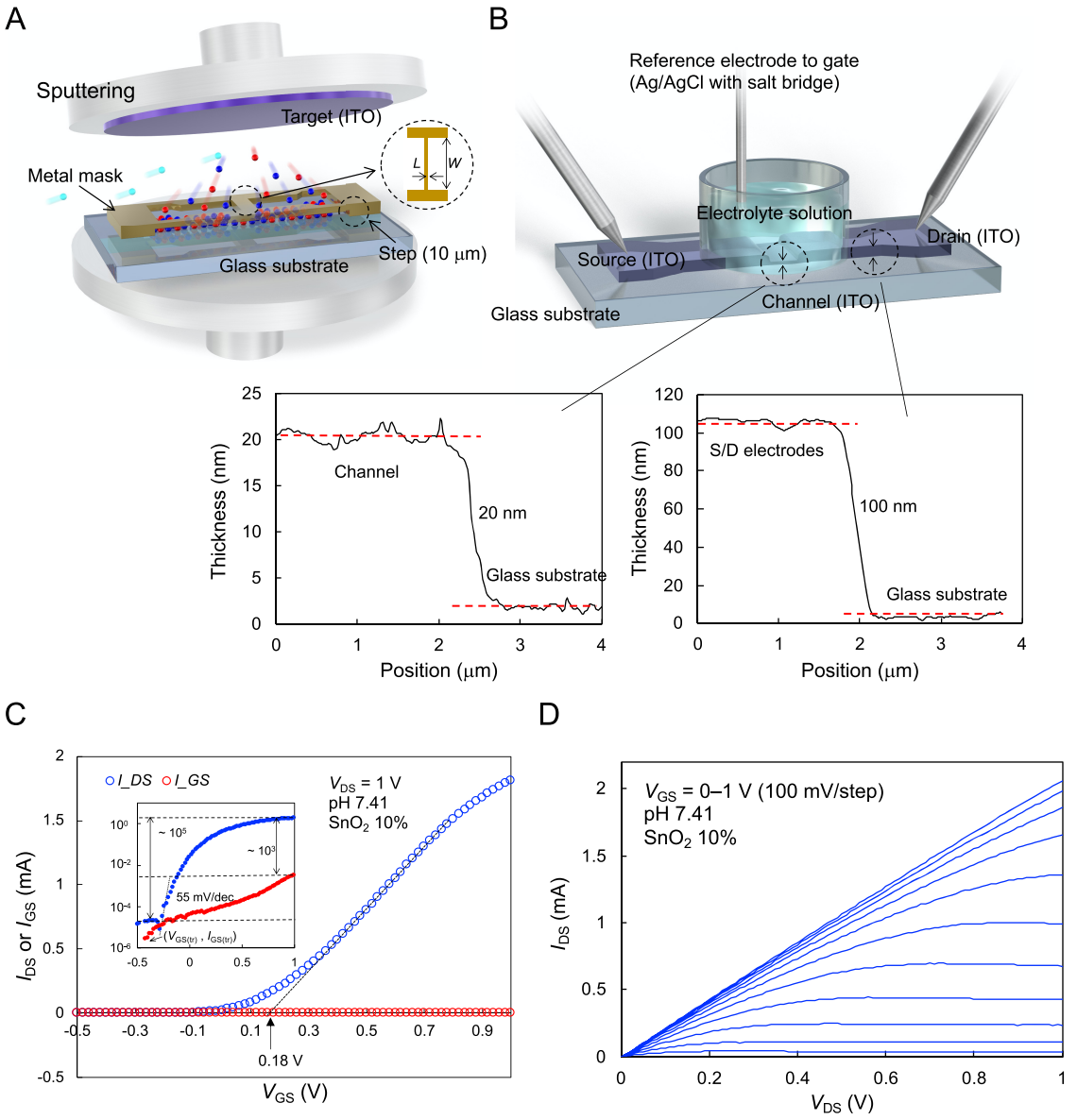

Figure 1. Fundamental features of the solution-gated ultrathin channel ITO-based FET sensor fabricated by the one-step procedure. (A) One-step sputtering with controlled metal shadow mask for the all-by-ITO technology. (B) Conceptual structure of the solution-gated ultrathin channel ITO-based FET sensor. The film thicknesses at/near the ITO channel and at ITO S/D electrodes were measured by AFM. (C) I_{DS}–V_{GS} and I_{GS}–V_{GS} transfer characteristics in the phosphate buffer solution (pH 7.41). V_{DS} was set at a constant 1 V. (D) I_{DS}–V_{DS} transfer characteristic in the phosphate buffer solution (pH 7.41). V_{GS} was applied at 100 mV/step from 0 to 1 V. In (B), (C), and (D), the target of ITO with 10 wt % SnO_2 was sputtered for 25 min using the metal shadow mask with the 10 μm sheet by the one-step procedure.

which was more than the extrinsic Debye length, that is, the screening length of Coulomb scattering,[24−26] the electrical communication between the source and drain (S/D) electrodes was induced by a very small density of free electrons in the depletion region, resulting in a clear on/off state of FETs. Thus, 2D-material FETs, the channel thickness of which is controlled to be approximately less than the depletion width, are expected to be highly sensitive in detecting of biomolecules that attach to the channel in a solution because multilayered bulk channels can easily form the electrical communication between S/D electrodes without being affected by surface charges. That is, a solution-gated 2D-channel FET biosensor, the channel of which is directly in contact with an electrolyte solution, is expected to have a steep subthreshold slope (SS), resulting in an ultrahighly sensitive biosensing owing to a relatively large capacitance of the electric double layer at the electrolyte solution/channel interface.

Among such semiconductive materials, we focus on a thin-film ITO with a thickness less than 30 nm, which is useful as the channel of a solution-gated 2D-channel FET biosensor. In a previous work, an active transistor based on an ultrathin ITO channel (down to 4 nm) with an ultrasmall equivalent oxide thickness (EOT) of 0.8 nm was fabricated for next-generation low-cost, low-power electronics.[27] This achievement can be explained from the fact that the reduction in channel thickness contributed to bandgap increase and free-carrier depletion in the same way as in 2D materials. Similarly, a 20-nm-thick ITO channel fabricated by direct imprinting using a quartz mold worked well for ferroelectric-gate thin-film transistors (FeTFTs).[28] In this case, ferroelectric-gate insulators such as

https://doi.org/10.1021/acsami.1c05830
ACS Appl. Mater. Interfaces XXXX, XXX, XXX−XXX

$(Bi,La)_4Ti_3O_{12}$ were suggested to induce free-carrier depletion in the thin-film ITO channel. Moreover, the back-gated ITO thin-film transistor showed a change in the field-effect mobility (~5 cm^2/Vs) for the adsorption of viruses.[29] In these back-gated ITO-based FETs, however, metal lines were unintentionally used as the gate electrode contacted with insulators; that is, their device structures were not intended for solution-gated FETs.

In addition, the fabrication procedure for FET devices is complicated; it involves photolithography to pattern electrodes and the deposition of electroactive materials on several parts. That is, a simpler fabrication process could accelerate the application of various semiconductive materials for biosensing devices and enable mass production for commercial application. Needless to say, a one-step procedure with a modified metal shadow mask proposed in this study simultaneously and simply provides a thin channel and thick S/D electrodes during sputtering, which result in the absence of interfacial traps among their electrodes in solution-gated 2D-channel FETs that also contributes to a steep SS.

Here, we propose a very easy fabrication process, that is, a one-step procedure for producing the solution-gated 2D-channel FET biosensor, focusing on the fully depleted ultrathin ITO channel. The solution-gated ultrathin channel ITO-based FET developed in this study exhibits various superior performances such as a steep SS and stable ion responsivity. Moreover, we find the possibilities of biological sensing using our new device fabricated by this one-step procedure, which has a great future potential in bioelectronics.

2. RESULTS AND DISCUSSION

2.1. Rapid and Easy Process to Fabricate a Solution-Gated FET and Its Fundamental Electrical Properties. A one-step procedure for fabricating a solution-gated FET with an ultrathin ITO channel is proposed here for ion and biological sensing. The metal shadow mask shown in Figure 1A (Figure S1) was prepared for sputtering the ITO film. The metal shadow mask included two regions cut out for the sputtered S/D electrodes. The channel width (W) and length (L) in the metal shadow mask were 3000 and 100 μm, respectively. Moreover, 10-μm-thick sheets were placed on both ends of the metal shadow mask, which were contacted with a glass substrate. This means that the bottom of the metal shadow mask corresponding to the channel was raised to 10 μm from the substrate; as a result, the creeping of some particles into the gap was induced while sputtering. Consequently, a thinner ITO channel and thicker ITO S/D electrodes were formed on the substrate during the one-step sputtering. The fabricated device was treated in an electrolyte solution, where a Ag/AgCl reference electrode with a salt bridge and the channel and part of S/D electrodes were immersed (Figure 1B). That is, the thin ITO channel also worked as an ion-sensitive membrane, owing to the intrinsic oxidated surface directly contacting with an electrolyte solution, without the need to apply an additional coating with oxide insulators such as SiO_2 on the channel. In fact, the thicknesses of the channel and the S/D electrodes, which were formed by sputtering for 25 min using the 10 wt % SnO_2–ITO target, were measured by AFM to be approximately 20 and 100 nm, respectively. Also, a slope was formed between the channel and the S or D electrode owing to the wraparound of particles sputtered into the gap, showing an approximately 45 nm thickness at the position a few tens of μm away from the channel (Figure S2). Moreover, Figure 1C,D shows the I_{DS}–V_{GS} and I_{DS}–V_{DS} transfer characteristics at pH 7.41 for the solution-gated FET with the 20-nm-thick ITO channel obtained by the one-step procedure. The thickness of S/D electrodes (about 100 nm) was sufficient to retain their electrical conductivities. This device showed the clear electrical properties of transistors. The ratio of the on-state to off-state current (I_{on}/I_{off}) at V_{DS} = 1 V was in the range of 10^5–$10,^6$which was not as high as that measured under vacuum without solutions ($I_{on}/I_{off} > 10^9$ at V_{DS} = 1 V) in a previous work, whereas the SS was calculated to be 55 mV/dec, which is comparable to that obtained in a previous study.[27] Also, the leakage current I_{GS} and I_{DS}/I_{GS} were mentioned later.

Figure 2 shows the maximum conductivity (σ_{max}) and I_{on}/I_{off} in the phosphate buffer solution (pH 7.41) as functions of the thickness of the ITO channel using the solution-gated ITO-based FET obtained by the one-step procedure. The thickness of the ITO channel was controlled by changing the sputtering time for the metal shadow mask with sheets of different thicknesses (Figure S3). When the thickness of the ITO channel was smaller than ~30–40 nm, which was assumed to be near the maximum depletion thickness (t_{Dm}) of the ITO channel, I_{on}/I_{off} was clearly found to be ~10.[5] That is, the ultrathin film of ITO (less than 30–40 nm) contributed to the bandgap increase and free-carrier depletion and then provided the transistor properties. In the case of a thicker ITO channel of more than 30–40 nm, the electrical communication between the S/D electrodes occurred below the depletion region, depending on V_{DS}. t_{Dm} can be calculated using eq 1, which is based on the screening length (λ_{SL}) derived from the extrinsic Debye length (λ_D).[23]

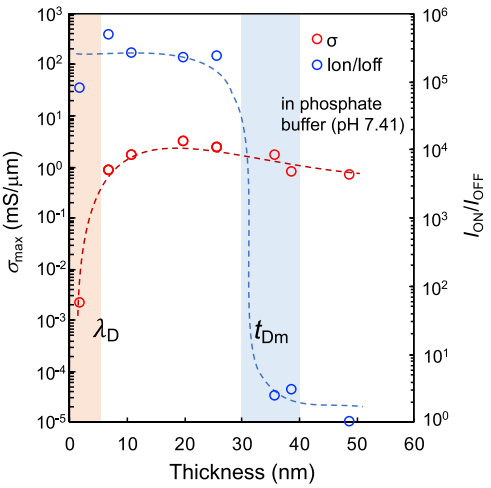

Figure 2. Ratio of on-state to off-state current (I_{on}/I_{off}) and maximum conductivity (σ_{max}) with changing thickness of the ITO channel. The target of ITO with 10 wt % SnO_2 was sputtered according to Figure S3 to control the channel thickness. I_{on}/I_{off} was calculated from the ratio of the maximum I_{DS} (at V_{GS} = 1) to the off-state I_{DS} in the I_{DS}–V_{GS} transfer characteristic (V_{DS} = 1 V) in the phosphate buffer solution (pH 7.41). σ_{max} was derived from the maximum I_{DS} (at V_{GS} = 1) and the device structure. The film thickness at the ITO channel was measured by AFM and 3D laser scanning confocal microscopy. The maximum depletion thickness (t_{Dm}) of the ITO channel was determined from the data points of I_{on}/I_{off}, and the extrinsic Debye length (λ_D) was calculated using eq 2.

https://doi.org/10.1021/acsami.1c05830
ACS Appl. Mater. Interfaces XXXX, XXX, XXX–XXX

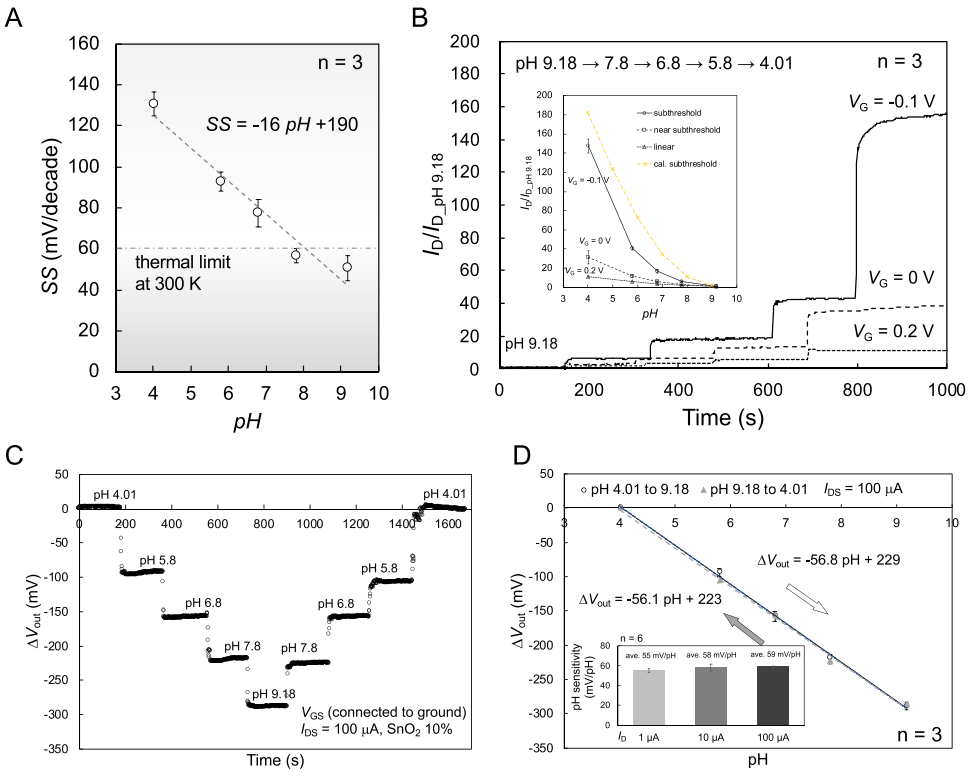

Figure 3. Electrical properties of the solution-gated ultrathin channel ITO-based FET sensor at various pHs (4.01, 5.8, 6.8, 7.8, and 9.18). The target of ITO with 10 wt % SnO_2 was sputtered for 25 min using the metal shadow mask with the 10-μm-thick sheet by the one-step procedure. Error bars represent the standard deviation determined from the number of experiments (n = 3 at each pH). (A) Subthreshold slope (SS) as a function of pH. (B) Real-time monitoring of I_{DS} at V_{GS} = −0.1 V (subthreshold regime), V_{GS} = 0 V (near-subthreshold regime), and V_{GS} = 0.2 V (linear regime) with change in pH. The inset shows each calibration curve, where that calculated using eq 6 is plotted. (C) ΔV_{out} at various pHs of solutions measured using the source-follower circuit. The Ag/AgCl reference electrode was connected to the ground. I_{DS} was set to be 100 μA. (D) Calibration curve of ΔV_{out} as a function of pH (circles from 4.01 to 9.18, triangles from 9.18 to 4.01). These were obtained from the data obtained in (C). In the inset, the pH sensitivities based on ΔV_{out} were demonstrated for the difference in I_{DS} (1, 10, and 100 μA).

$$t_{Dm} = \lambda_{SL} = \sqrt{\frac{4\varepsilon_{ITO}k_BT\ln\left(\frac{N_D}{n_i}\right)}{e^2N_D}} \quad (1)$$

$$\lambda_D = \sqrt{\frac{\varepsilon_{ITO}k_BT}{e^2N_D}} \quad (2)$$

Here, N_D, n_i, ε_{ITO}, k_B, T, and e are the density of donors, the intrinsic carrier density, the dielectric constant of ITO, the Boltzmann constant, the temperature, and the elementary charge, respectively. In particular, N_D is related to the composition of SnO_2 doped in In_2O_3. The concentration profile of Sn and In atoms around the ITO channel was measured by energy-dispersive X-ray spectroscopy (EDS) (Figure S4). A 10 wt % SnO_2−ITO target was sputtered on the glass substrate by the one-step procedure. The concentration of Sn atoms was almost maintained as about 10 wt % at the S/D electrodes, whereas that at the channel increased to about 15 wt %, which resulted from the creeping of particles into the gap between the metal shadow mask and the substrate during sputtering. This compositional change was assumed because there were intrinsic and extrinsic factors for the creeping of particles into the gap during sputtering, namely, the difference in molar mass between In_2O_3 (277.63) and SnO_2 (150.71) and the electric field generated in the gap between the metal shadow mask (stainless steel) and the glass substrate with electrons generated in sputtering. As a result, the donor density was assumed to be higher in the channel. Using eq 1, we can calculate N_D to be approximately $2 - 3 \times 10^{24}$ cm^{-3}, considering $n_i \approx 1 \times 10^{18}$ cm^{-3} (carrier density of undoped In_2O_3)[30] and $t_{Dm} \approx 30 - 40$ nm obtained in Figure 2. Moreover, σ_{max} markedly increased with the increasing thickness of the ITO channel and was saturated at the channel thickness of more than $\lambda_D \approx 4 - 5$ nm, which was in good agreement with that calculated using eq 2. If the channel thickness was smaller than λ_D, the electrical communication would have been prevented by Coulomb scattering because most 2D materials are intrinsically charged by defects and impurities.[24−26] On the other hand, the S/D electrodes required a larger thickness of several tens of nm than the channel to maintain their electrical conductivities (Figure S3). Thus, the solution-gated FET with the ultrathin film ITO channel, which was simply fabricated by the one-step procedure, showed transistor properties similar to those of 2D materials.

The solution-gated FET with the 20-nm-thick ITO channel exhibited a remarkably steep SS (Figure 1C), which was very close to the thermal limit (60 mV/dec at 300 K) and may result in a steep SS of less than 60 mV/dec in 2D-FETs.[31−33] The SS of the developed device was fivefold lower (more superior) than that of a silicon-based ion-sensitive FET (ISFET) (Figure S5A,B). Since this device was fabricated by the one-step procedure, the effect of interfacial traps among electrode materials on SS was neglected, unlike in other 2D-FETs.[31,32] The capacitance of oxide hypothesized on the

https://doi.org/10.1021/acsami.1c05830
ACS Appl. Mater. Interfaces XXXX, XXX, XXX−XXX

channel (C_{ox}) could be infinitely large (oxide thickness, $t_{ox} \rightarrow 0$) in this case when assuming SS = $\ln(10)\frac{kT}{q}\cdot[1 + (C_s + C_{it})/C_{ox}]$,[33,34] where C_s is the depletion layer capacitance (ITO channel) and $\frac{kT}{q}$ is the thermal voltage. Here, the presence of a significant interface-trap density D_{it}, that is, its associated capacitance C_{it} ($=q^2D_{it}$), is considered[34] because the electrolyte solution/ITO channel interface was considered as a chemically active site even in the absence of interfaces among the electrodes in solution-gated ITO-channel FETs fabricated by the one-step procedure. Here, instead of C_{ox}, the electric double-layer capacitance (C_{dl}) can be assumed because of the absence of C_{ox} for the solution-gated 20-nm-thick ITO channel in this study. Not only is C_{dl} relatively large at the oxide/solution interface (1−100 μF/cm^2),[35] it also depends on the charges of hydroxy groups at the ITO channel, which vary with pH. That is, when C_{dl} is relatively large and C_{it} varies with the change in pH across the isoelectric point of ITO (pI 7−8.5)[36,37] in a circuit, a steep SS of approximately 60 mV/dec or lower is expected according to SS = $60\cdot[1 + (C_s + C_{it})/C_{dl}]$ at T = 300 K. This was shown by the finding that SS changed depending on pH, as shown in Figure 3A. The increase in the pH of the measurement solutions contributed to the steep SS, showing the thermal limit to be around pH 7−8 near pI. This is because the charges of hydroxy groups at the ITO channel changed from positive in acidic solutions to neutral in neutral solutions, whereby C_{it} would have decreased with increasing pH, in addition to the effect of the originally large C_{dl}. That is, D_{it} was assumed to be larger in acidic solutions owing to the positively charged hydroxy groups at the ITO channel surface than in neutral solutions, whereas the change in C_{dl} (ΔC_{dl}) with pH would not have been so significant; that is, ΔC_{dl} with pH was not so large at an oxide/solution interface, although C_{dl} decreased with increasing pH in a previous study.[38] In addition, the charges of hydroxy groups at the ITO channel should have been negative in an alkaline solution with pH 9.18 at higher than pI. The charge shift in the alkaline solution at the ITO channel across pI may have contributed to a subthermal limit steep SS. However, the changes in C_{dl}, C_{it}, and C_s based on the charge shift, that is, the mechanism underlying the sub-60 mV/dec steep SS in the solution-gated ITO-channel FET, should be further investigated in the future in reference to previous studies. As examples, one study showed that a negative capacitance in a ferroelectric (FE) gate insulator induced a sub-60 mV/dec steep SS.[39] Another study showed that the polarization reversal in an oxide film via the electric double layer, which was formed on the basis of positively or negatively charged ions, was also controlled in an ionic liquid in contact with the oxide film.[40] Also, the sensitivity of nanowire-FET sensors was exponentially enhanced in the subthreshold regime in a previous work.[41] This means that the highly sensitive detection of ions and biomolecules with charges is expected using the devices with much better SS. Considering the SS shown in Figure 3A, I_{DS}^{pH} was continuously monitored with changing pH at a constant $V_{GS\_sub}^{pH}$ (−100 mV) in the subthreshold regime, $V_{GS\_nsub}^{pH}$ (0 mV) in the near-subthreshold regime, or $V_{GS\_lin}^{pH}$ (200 mV) in the linear regime, as shown in Figure 3B. $I_{DS\_sub}^{pH\ 9.18}$ was obtained at $V_{GS\_sub}^{pH\ 9.18}$ (pH 9.18), and the ratio $|I_{DS}^{pH}/I_{DS\_sub}^{pH\ 9.18}|$ was plotted. $I_{DS}^{pH}$was offset with $I_{DS\_sub}^{pH\ 9.18}$. $|I_{DS}^{pH}/I_{DS\_sub}^{pH\ 9.18}|$ in the subthreshold regime was clearly larger than $|I_{DS}^{pH}/I_{DS\_nsub}^{pH\ 9.18}|$ and $|I_{DS}^{pH}/I_{DS\_lin}^{pH\ 9.18}|$ in the near-subthreshold and linear regimes for the change in pH (ΔpH). ΔpH induced the change in the interfacial potential (ΔV_{out}) corresponding to the change in the charges of hydroxy groups based on the equilibrium reaction with hydrogen ions. This means that V_{GS}^{pH} was additively applied from $V_{GS\_sub}^{pH\ 9.18}$ by ΔpH in the circuit; therefore, $|I_{DS}^{pH}/I_{DS\_sub}^{pH\ 9.18}|$ largely changed owing to ΔpH depending on SS compared with the current ratios in the other regimes. I_{DS}^{pH} in the subthreshold regime is expressed by SS:

$$\log_{10}\left|\frac{I_{DS}^{pH}}{I_{DS\_sub}^{pH\ 9.18}}\right| = \frac{V_{GS}^{pH} - V_{GS\_sub}^{pH\ 9.18}}{SS} \quad (3)$$

As SS depended on ΔpH (Figure 3A), eq 3 is modified to

$$\log_{10}\left|\frac{I_{DS}^{pH}}{I_{DS\_sub}^{pH\ 9.18}}\right| = \frac{V_{GS}^{pH} - V_{GS\_sub}^{pH\ 9.18}}{-16\ pH + 190} \quad (4)$$

Moreover, oxide membranes such as ITO cause the Nernstian response in electrolyte solutions, that is, ΔV_{out} (or ΔV_T) for ΔpH (ΔV_{Ner}) at the solution/oxide interface (see Figure 3C,D below). Therefore, ΔV_{Ner} is expressed as

$$\Delta V_{Ner} = \frac{V_{GS}^{pH} - V_{GS\_sub}^{pH\ 9.18}}{|pH - pH_{sub}|}, \quad (5)$$

where pH_{sub} was set as 9.18 in this study. From eqs 4 and 5, eq 6 is derived as

$$\left|\frac{I_{DS}^{pH}}{I_{DS\_sub}^{pH\ 9.18}}\right| = 10^{\Delta V_{Ner}\,|pH-9.18|/-16\ pH+190}. \quad (6)$$

Indeed, $|I_{DS}^{pH}/I_{DS\_sub}^{pH\ 9.18}|$ in the subthreshold regime exponentially increased (inset in Figure 3B). In addition, the ideal curve calculated from eq 6 conceptually matched the data obtained (inset in Figure 3B). Thus, the electrical signals measured in the subthreshold regime were about 10 times larger than those measured in the linear regime, which would contribute to the ultrasensitive detection of biomolecules. On the other hand, the change in the interfacial potential ΔV_{out} between the measurement solution and the ITO channel for the one-step-fabricated device was also measured with changing pH at a constant I_{DS} = 100 μA in the linear regime using the source-follower circuit. As shown in Figure 3C,D, the pH response was very rapid, showing the same behavior as that of the silicon-based ISFET (Figure S5C,D). The pH sensitivity was calculated to be about 56 mV/pH, showing the ideal one near the Nernstian response (ΔV_{Ner} = 59.2 mV/pH at 25 °C). The stepwise response of ΔV_{out} with increasing pH from 4.01 to 9.18 reproducibly returned back to the original state with decreasing pH from 9.18 to 4.01. The pH sensitivity was similarly obtained from the shift in the threshold voltage (V_T) in the transfer characteristics as well (Figure S6). Moreover, the pH sensitivity almost showed the Nernstian response even when measured in the subthreshold regime at I_{DS} = 1 μA and the near-subthreshold regime at I_{DS} = 10 μA (inset in Figure 3D). This is because ΔV_{out} strongly depended on the equilibrium reaction at the ITO channel surface rather than the semiconducting properties. Thus, ΔV_{Ner} was obtained from the linear relationship between ΔV_{out} (or ΔV_T) and ΔpH, whereas I_{DS}^{pH} was exponentially changed with ΔpH, as determined using eqs 5 and 6, respectively. However, when sheets of 20 μm thickness were used to raise the bottom of the metal shadow mask for sputtering, the off-state region was not

https://doi.org/10.1021/acsami.1c05830
ACS Appl. Mater. Interfaces XXXX, XXX, XXX−XXX

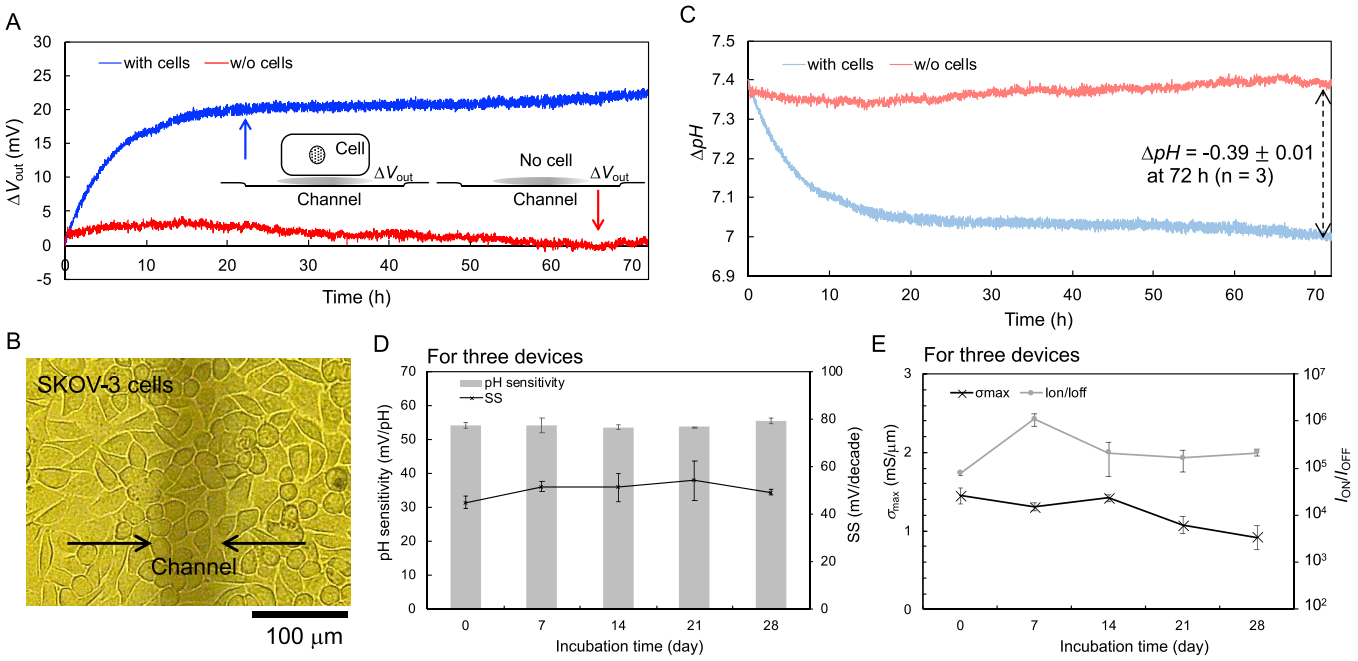

Figure 4. Stability of electrical properties of the solution-gated ultrathin channel ITO-based FET sensor. The target of ITO with 10 wt % SnO_2 was sputtered for 25 min using the metal shadow mask with the 10-μm sheet by the one-step procedure. (A) ΔV_{out} of solution-gated ultrathin channel ITO-based FET sensors with and without SK-OV-3 cells. The cells were precultured on the ITO channel for 24 h before the electrical measurement, and then the culture medium was replaced with a fresh one at 0 h of the measurement to replenish nutrients such as glucose. As a control sensor, a device without cell culture was prepared, and the exchange of culture medium was performed in the same way as the device with cell culture. (B) Photograph of SK-OV-3 cells cultured on the ITO channel under an inverted microscope. (C) Change in pH induced by cellular respiration. ΔpH was calculated from ΔV_{out} obtained in (A) according to the pH sensitivity of 56 mV/pH (see Figure 3D). The initial pH of the culture medium was 7.4. ΔpH at 72 h was averaged from three devices with standard deviation. (D) Stability of pH sensitivity and subthreshold slope (SS) with incubation time (0−28 days). Three devices were utilized for the evaluation with standard deviation. (E) Stability of the ratio of on-state to off-state current (I_{on}/I_{off}) and maximum conductivity (σ_{max}) for incubation time (0−28 days). Three devices were utilized for the evaluation with standard deviation.

obtained and I_{DS} linearly increased for any V_{GS} applied with increasing V_{DS} (Figure S7), depending on the sputtering time (Figure S3). The thickness of the ITO channel in this case was about 50 nm and larger than that obtained using the metal shadow mask with 10-μm-thick sheets. That is, a thickness down to around 30−40 nm is required for the depletion of the ITO channel (Figure 2). Also, no transistor characteristics were observed for the device sputtered using the uncontrolled mask without the sheet (Figure S8) because the channel itself was not formed. The above electrical characteristics of the solution-gated FET with the ultrathin 10 wt % SnO_2−ITO channel were similarly obtained even for 5 wt % SnO_2−ITO and 15 wt % SnO_2−ITO (Figure S9), although the sheet resistance of ITO was assumed to be minimum at 10 wt % SnO_2.[42] That is, I_{on}/I_{off} (~10^5), SS (~60 mV/dec), pH sensitivity (~56 mV/pH), and so forth at pH 7.41 did not largely change in the range of 5 to 15 wt % SnO_2. The dependence of the electrical properties on SnO_2 concentrations of less than 5 wt % or more than 15 wt % should be further investigated in the future. Although such attractive devices can be fabricated by a multistep procedure including photolithography (Figure S10), the electrical properties such as I_{on}/I_{off} and SS at pH 7.41 were inferior to those in the devices obtained by the one-step procedure (~10^5 → ~10^3 and 60 → 100 mV/dec). In particular, the deterioration of SS may be due to the interfacial effect between the channel and the S/D electrodes formed by the multistep procedure even when an ITO with the same composition (10 wt % SnO_2) was used for both of them. The reason may be because the electrical contacts formed by the multistep procedure between the channel and the S/D electrodes, which would have contributed to the Fermi level pinning effect, deteriorated those properties, whereas no contact was formed by the one-step procedure. On the other hand, the pH responsivity of the multistep-fabricated device (approximately 58 mV/pH in Figure S10C,D) was comparable to that of the one-step-fabricated device because it is derived from ΔV_{out} based on the equilibrium reaction between hydrogen ions and hydroxy groups at the ITO surface under constant I_{DS}.

In addition, the electrical behavior of I_{GS} was investigated to evaluate the device performances in solutions (Figure S11). The ratio of I_{DS} to I_{GS} (I_{DS}/I_{GS}) at V_{GS} = 1 V for the one-step-fabricated device was estimated to be approximately 10^3 at pH 7.41 (Figure 1C), which was sufficiently large to evaluate the electrical signals derived from the change in ionic or molecular charges, which was induced by chemical reactions; that is, I_{GS} was small to be sufficiently neglected regardless of pH (Figure S11A). Depending on the V_{GS} applied, I_{GS} was roughly generated on the basis of an electrical circuit with solution resistance (R_s), charge transfer resistance (R_{CT}), and C_{dl}. Both R_{CT} and C_{dl} depend on the intrinsic surface charges of the ITO channel derived from hydroxy groups; that is, they would vary with changing pH in measurement solutions. A transient gate voltage ($V_{GS(tr)}$) at a transient leakage current ($I_{GS(tr)}$), which was found as the minimum positive leakage current (Figure 1C and Figure S11B),may have depended on the pH. At pH 7.41, for instance, the positive I_{GS} appeared at around −0.44 V ($V_{GS(tr)}^-$) for the leading half of the sweep of V_{GS} (−1 to 1 V)

https://doi.org/10.1021/acsami.1c05830
ACS Appl. Mater. Interfaces XXXX, XXX, XXX−XXX

and disappeared at around 0.46 V ($V_{GS(tr)}^{+}$) for the trailing half of the sweep of V_{GS} (1 to −1 V), as shown in Figure S11B. Such $V_{GS(tr)}$ at $I_{GS(tr)}$ expectedly depended on ΔV_{out} in relation to C_{dl} at the channel surface. The ITO surface with hydroxy groups would have been positively or negatively charged with varying pHs on the border of the isoelectric point (pI 7−8.5).[36,37] Therefore, charged hydroxy groups should have contributed to $V_{GS(tr)}$ according to the pH of the measurement solutions, although the details need to be investigated in the future. On the other hand, I_{DS}/I_{GS} at V_{GS} = 1 V for the multistep-fabricated device was estimated to be approximately 10^1 at pH 7.41; I_{DS} was so small that I_{GS} could not be neglected (Figure S10A). Such leakage currents might damage cells, which were directly cultured on the ITO channel and S/D electrodes even when using the one-step-fabricated device, in the case where V_{GS} (= 2.5 V) was applied during electrical measurements (Figure S12). However, the real-time measurement during cell culture resulted in the change in pH at the cell/channel interface caused by cellular respiration over a relatively long term (see Section 2.2). This is because ΔV_{out} was output at V_{GS} = 0 V (connected to the ground to maintain a constant V_{GS}) under a constant I_{DS} with the source-follower circuit and then the effect of I_{GS} was suppressed.

2.2. Electrical Stability of the Ultrathin Channel ITO-Based FET Fabricated by the One-Step Procedure and Cell Monitoring. In general, the electrical characteristics of 2D materials are assumed to be unstable in a solution owing to oxidation at the surfaces.[43−45] That is, 2D materials are not directly immersed in a solution for long-term biosensing; thus, their surfaces are passivated by some insulators.[20] However, ITO thin films are relatively stable in a solution owing to their intrinsic oxidated surfaces. In this study, the electrical stability of the solution-gated ITO-FET with the 20-nm-thick ITO channel fabricated by the one-step procedure was determined by monitoring the cellular respiration activity in a cell culture medium. Figure 4A shows ΔV_{out} for SK-OV-3 cells cultured on the ITO channel using the solution-gated 20-nm-thick channel ITO-based FET sensor. Using this device, we found that ΔV_{out} gradually increased during the cell culture, whereas the control sensor without cells hardly changed during the electrical measurement. To stimulate the cells, the culture medium was changed with a fresh one at 0 h (i.e., at the start of measurement), resulting in the replenishment of nutrients such as glucose. These cells cultured on the ITO channel were alive even after the electrical measurement for 72 h (Figure 4B). Since the fabricated devices by the one-step procedure were transparent because they were completely made of ITO, the cell morphologies were clearly observed under an inverted microscope, similarly to the observation of cells cultured on a cell culture dish. This means that information on cellular functions that cannot be obtained by electrical measurements can be simultaneously obtained using a fluorescence microscope for cell imaging in the future.[46] The increase in ΔV_{out} resulted from the increase in the concentration of hydrogen ions with positive charges at the ITO channel surface, that is, the cell/channel nanogap interface, generated by cellular respiration. Such electrical measurements of cellular respiration have been reported in a previous work.[14] That is, the change in pH induced by carbon dioxide generated by cellular respiration was detected at the cell/gate insulator interface using the solution-gated ISFET. This was confirmed by fluorescence imaging at the nanogap interface between the adhered cells and the gate substrate.[15] Moreover, the solution-gated ITO-FET with the ultrathin channel showed the ideal responsivity to the change in pH, similar to that of ISFET sensors, as shown in Figure 3. Therefore, ΔV_{out} shown in Figure 4A demonstrated the change in pH induced by cellular respiration (Figure 4C). ΔV_{out} was translated to ΔpH, considering that the initial pH value of the culture medium used was 7.4 and the pH responsivity of the devices was approximately 56 mV/pH (Figure 3C,D). Thus, ΔpH at the cell/channel nanogap interface was calculated to be −0.39 ± 0.01 at 72 h; that is, the long-term electrical stability of the solution-gated ITO-FET with the ultrathin ITO channel was confirmed from the electrical measurement of cellular respiration. Furthermore, the electrical stability was also evaluated from the pH sensitivity and SS measured every week using the solution-gated ITO-FET with the 20-nm-thick ITO channel obtained by the one-step procedure (Figure 4D,E and Figure S13). The pH sensitivity and SS of the devices used were maintained in the range of 53−55 mV/pH and 50−60 mV/dec (pH 7.8) even when the devices were immersed in the buffer solution (pH 7.41) for 1 month (Figure 4D). In particular, the shift in V_{out} (or V_{GS}) at a constant I_{DS} resulted from that in the interfacial potential at the solution/channel interface, that is, the change in the ionic charges based on the equilibrium reaction between hydrogen ions and hydroxy groups; thus, the pH sensitivity obtained by the source-follower circuit was maintained in the solution for a long time. This indicates that the surface of the ITO channel was stably ionized while immersed in the solution (pH 7.41), although such a surface condition may depend on the pH of the solution used. The electrical stability was based on the intrinsic surface properties of ITO in contact with the solution, whereas the problem about whether cells survived or not during the electrical measurement was solved by using the source-follower circuit that did not largely contribute to I_{GS} (V_{GS} = 0). Similarly, I_{on}/I_{off} and σ_{max} did not deteriorate, remaining at ∼10^5 and ∼1 mS/μm, respectively, for 1 month, as shown in Figure 4E. However, such performances might deteriorate after the device is immersed in the solution for more than 1 month because σ_{max} appeared to decrease slightly from around day 21. This may be because the deterioration rate of the ITO films in solutions is basically larger than that in air owing to their slight solubility,[47] and then the concentration of oxygen vacancies gradually changes.

3. CONCLUSIONS

In this study, the solution-gated ITO-based FET sensor with the ultrathin channel was fabricated by a one-step procedure, which contributed to the all-by-ITO technology. This was simply realized by using the metal shadow mask with thin sheets at both ends because the bottom of the metal shadow mask corresponding to the channel became slightly raised from the substrate owing to the thin sheets and then some particles crept into the gap during sputtering. The 20-nm-thick ITO channel resulted in the bandgap increase and free-carrier depletion in the same way as in 2D materials. The threshold thickness of the depleted ITO channel was determined to be ∼30−40 nm from the significant change in I_{on}/I_{off}. The remarkably steep SS was derived from the interfacial trap-free structure based on the one-step fabrication as well as the relatively large capacitance of C_{dl} based on the direct contact of electrolyte solutions with the ITO channel, and caused the exponential pH sensitivity in the subthreshold regime. This is why we can expect the highly sensitive detection of ions and biomolecules with charges in the subthreshold regime using

https://doi.org/10.1021/acsami.1c05830
ACS Appl. Mater. Interfaces XXXX, XXX, XXX−XXX

the solution-gated ultrathin channel ITO-based FET sensor. Moreover, SS strongly depended on pH and particularly showed the thermal limit at around the isoelectric point of the ITO surface. On the other hand, the change in the interfacial potential at the electrolyte solution/ITO channel clearly showed the Nernstian response as the pH sensitivity. Since this was due to the change in ionic charges based on the equilibrium reaction between hydrogen ions and hydroxy groups at the ITO channel surface, the potentiometric measurement may contribute to the electrical detection of biomolecular recognition events at the solution/channel interface regardless of semiconducting properties. Moreover, the electrical stabilities of the solution-gated ultrathin channel ITO-based FET sensor were confirmed from the pH sensitivity, SS, I_{on}/I_{off}, and σ_{max}, which were almost maintained in the buffer solution for 1 month, as well as the long-term monitoring of cellular functions. This one-step procedure makes a significant contribution to not only the enhancement of the performance of solution-gated 2D-channel FET biosensors but also the mass production for commercial applications owing to its easy process when considering the development of ion and biological sensors in the future.

4. MATERIALS AND METHODS

4.1. ITO Film in One-Step Sputtering. The ITO thin film in this study was fabricated on a glass substrate under 20% Ar atmosphere (without O_2) using a radiofrequency (RF) sputtering system (ULVAC, Inc.). The metal shadow mask made of stainless steel was fabricated by wire electric discharge machining. The mask sizes were designed to deposit the ITO film for the S/D electrodes and the channel in the one-step sputtering. In particular, the bottom of the metal shadow mask corresponding to the channel was raised to 10 and 20 μm from the substrate so that the creeping of some particles into the gap between the mask for the channel and the glass substrate occurred during sputtering. To control the thicknesses of the ITO channel and S/D electrodes, the sputtering time was changed from 5 to 25 min using the designed mask with the 10 or 20 μm gap. The thickness of the ITO film was measured by atomic force microscopy (AFM; Agilent Technologies) and 3D laser scanning confocal microscopy (VK-X3000, Keyence). The width (W) and length (L) of the gate channel were ideally 3000 and 100 μm, respectively, which were based on the size of the metal shadow mask. Actually, the average length of the deposited channels was measured as 100 ± 15 μm using a laser microscope, which was the distance between the ends of S/D electrodes with flatness, considering the slope between the channel and the S/D electrodes. The concentration profiles of In and Sn atoms around the ITO channel and S/D electrodes were measured by energy-dispersive X-ray spectroscopy (EDS).

4.2. Electrical Measurement of the Solution-Gated Ultrathin Channel ITO-Based FET in an Electrolyte Solution. The sensing surface, onto which measurement solutions were poured, was separated from the connection by the encapsulation with a polycarbonate ring (6 mm diameter) and a resin (polydimethylsiloxane). The $I_{DS}-V_{GS}$ and $I_{DS}-V_{DS}$ transfer characteristics of the solution-gated ultrathin channel ITO-based FET were measured within −1 to 1 V while changing the pH from 4.01 to 9.18 using a semiconductor parameter analyzer (B1500A, Agilent Technologies). Phosphate buffer solutions were prepared with pHs from 5.8 to 7.8 by controlling the mixing ratio of Na_2HPO_4 to KH_2PO_4 (Wako Pure Chemical Industries, Ltd.). Also, the standard buffer solutions with pHs of 4.01, 7.41, and 9.18 (Wako Pure Chemical Industries, Ltd.) were prepared. From these transfer characteristics, $V_{GS\_sub}^{pH}$, $V_{GS\_nsub}^{pH}$, and $V_{GS\_lin}^{pH}$ in the subthreshold, near-subthreshold, and linear regimes were determined. In particular, $V_{GS\_sub}^{pH}$, $V_{GS\_nsub}^{pH}$, and $V_{GS\_lin}^{pH}$ at pH 9.18 were utilized as the constant biases ($V_{GS\_sub}^{pH\ 9.18}$, $V_{GS\_nsub}^{pH\ 9.18}$, and $V_{GS\_lin}^{pH\ 9.18}$) for evaluating the change in I_{DS}^{pH} because the $I_{DS}-V_{GS}$ transfer curve shifted in the positive direction with increasing pH and then I_{DS}^{pH} could be shifted in the positive direction with decreasing pH. To evaluate the basic electrical signal, the shift in the threshold voltage ΔV_T was defined as the difference in V_G at a constant I_D in the $I_{DS}-V_{GS}$ transfer characteristics. The surface potential at the gate surface (interfacial potential V_{out}) in the above buffer solutions was monitored using a source-follower circuit[48] with which the change in the gate surface potential could be read out directly at a constant I_D. In this study, V_{DS} and I_D were set to be 1 V and 10−100 μA, respectively. The long-term stability of solution-gated ultrathin channel ITO-based FETs was evaluated once a week for 1 month from the pH sensitivity based on the change in V_{out} (ΔV_{out}) at various pHs and some parameters (SS, σ_{max}, and I_{on}/I_{off}) of the $I_{DS}-V_{GS}$ transfer characteristics. For the evaluation of the long-term stability, three devices were immersed in the phosphate buffer solution (pH 7.41) for 1 month.

4.3. Cell Culture on the ITO Channel. SK-OV-3 (ovarian cancer cell line) cells were cultured on the transparent ITO channel at 37 °C and 5% CO_2 in an incubator system (ASTEC Co., Ltd.) to investigate the electrical properties of cells using the ultrathin channel ITO-based FET sensor. Dulbecco's modified Eagle's medium (DMEM, Invitrogen) (+1% FBS) was utilized as the culture medium. The cells were seeded on the channel in a culture well of 300 μL volume at a concentration of about 1×10^5 cells/mL. The sensor was set up on the stage of the microscope in the incubator system. The electrical measurement was performed under suitable conditions for cell culture in the incubator system. After confirming that the cells were confluent, the change in V_{out} was monitored using the source-follower circuit. A few hundred cells adhered to the ITO channel area. Cellular respiration was activated by adding a fresh culture medium. The electrical signal for the target sample was evaluated by the differential measurement between the sample and the control sensors, which was performed to eliminate common background noises such as changes in temperature and ion concentration, and nonspecific adsorption.[49] Two types of the device were prepared for the differential measurement: one was an ultrathin channel ITO-based FET sensor with cells; the other was a control ultrathin channel ITO-based FET sensor without cells. SK-OV-3 cells were precultured on the ITO channel for 24 h, and then the culture medium was exchanged for both sensors at 0 h. In this study, the differential measurements were performed simultaneously using these two devices under the same conditions in the same incubator.

■ ASSOCIATED CONTENT

Supporting Information

The Supporting Information is available free of charge at https://pubs.acs.org/doi/10.1021/acsami.1c05830.

Metal shadow mask with steps (Figure S1); cross section of the ITO channel fabricated by the one-step procedure (Figure S2); control of channel thickness for sputtering time and thickness of sheet (Figure S3); concentration profile of Sn and In atoms around the ITO channel measured by energy-dispersive X-ray spectroscopy (EDS) (Figure S4); fundamental electrical properties of a conventional solution-gated silicon-based ion-sensitive FET (ISFET) (Figure S5); $I_{DS}-V_{GS}$ transfer curve for the change in pH (Figure S6); $I_{DS}-V_{GS}$ transfer curve of the solution-gated ITO-based FET with a thicker ITO channel (Figure S7); $I_{DS}-V_{GS}$ and $I_{GS}-V_{GS}$ transfer curve of the solution-gated ITO-based FET fabricated using a metal shadow mask without sheet (Figure S8); electrical characteristics of the solution-gated ultrathin channel ITO-based FET with different SnO_2 compositions (Figure S9); electrical characteristics of the solution-gated ultra-thin channel ITO-based FET fabricated by the multistep procedure (Figure S10); fundamental properties of the leakage current I_{GS} (Figure S11); effect of the leakage current on cellular

https://doi.org/10.1021/acsami.1c05830
ACS Appl. Mater. Interfaces XXXX, XXX, XXX−XXX

analysis (Figure S12); and electrical stability of the solution-gated ultrathin channel ITO-based FET sensor (Figure S13) (PDF)

AUTHOR INFORMATION

Corresponding Author

Toshiya Sakata − *Department of Materials Engineering, School of Engineering, The University of Tokyo, Tokyo 113-8656, Japan;* orcid.org/0000-0003-1246-5000; Email: sakata@biofet.t.u-tokyo.ac.jp

Authors

Shoichi Nishitani − *Department of Materials Engineering, School of Engineering, The University of Tokyo, Tokyo 113-8656, Japan*

Akiko Saito − *Department of Materials Engineering, School of Engineering, The University of Tokyo, Tokyo 113-8656, Japan*

Yuta Fukasawa − *Department of Materials Engineering, School of Engineering, The University of Tokyo, Tokyo 113-8656, Japan*

Complete contact information is available at: https://pubs.acs.org/10.1021/acsami.1c05830

Notes

The authors declare no competing financial interest.

ACKNOWLEDGMENTS

This study was partly supported by the Mirai Program of Japan Science and Technology (JST).

REFERENCES

(1) Bergveld, P. Development of an Ion-Sensitive Solid-State Device for Neurophysiological Measurements. *IEEE Trans. Biomed. Eng.* **1970**, *BME-17*, 70−71.

(2) Matsuo, T.; Wise, K. D. An Integrated Field-Effect Electrode for Biopotential Recording. *IEEE Trans. Biomed. Eng.* **1974**, *BME-21*, 485−487.

(3) Esashi, M.; Matsuo, T. Integrated Micro-Multi-Ion Sensor Using Field Effect of Semiconductor. *IEEE Trans. Biomed. Eng.* **1978**, *BME-25*, 184−192.

(4) Moss, S. D.; Janata, J.; Johnson, C. C. Potassium Ion-Sensitive Field Effect Transistor. *Anal. Chem.* **1975**, *47*, 2238−2243.

(5) Danielsson, B.; Lundström, I.; Mosbach, K.; Stiblert, L. On a New Enzyme Transducer Combination: The Enzyme Transistor. *Anal. Lett.* **1979**, *12*, 1189−1199.

(6) Souteyrand, E.; Cloarec, J. P.; Martin, J. R.; Wilson, C.; Lawrence, I.; Mikkelsen, S.; Lawrence, M. F. Direct Detection of the Hybridization of Synthetic Homo-Oligomer DNA Sequences by Field Effect. *J. Phys. Chem. B* **1997**, *101*, 2980−2985.

(7) Schöning, M. J.; Poghossian, A. Recent Advances in Biologically Sensitive Field-Effect Transistors (BioFETs). *Analyst* **2002**, *127*, 1137−1151.

(8) Sakata, T.; Miyahara, Y. Potentiometric Detection of Single Nucleotide Polymorphism Using a Genetic Field Effect Transistor. *ChemBioChem* **2005**, *6*, 703−710.

(9) Sakata, T.; Miyahara, Y. DNA Sequencing Based on Intrinsic Molecular Charges. *Angew. Chem., Int. Ed.* **2006**, *45*, 2225−2228.

(10) Ingebrandt, S.; Han, Y.; Nakamura, F.; Poghossian, A.; Schöning, M. J.; Offenhäusser, A. Label-Free Detection of Single Nucleotide Polymorphisms Utilizing the Differential Transfer Function of Field-Effect Transistors. *Biosens. Bioelectron.* **2007**, *22*, 2834−2840.

(11) Rothberg, J. M.; Hinz, W.; Rearick, T. M.; Schultz, J.; Mileski, W.; Davey, M.; Leamon, J. H.; Johnson, K.; Milgrew, M. J.; Edwards, M.; Hoon, J.; Simons, J. F.; Marran, D.; Myers, J. W.; Davidson, J. F.; Branting, A.; Nobile, J. R.; Puc, B. P.; Light, D.; Clark, T. A.; Huber, M.; Branciforte, J. T.; Stoner, I. B.; Cawley, S. E.; Lyons, M.; Fu, Y. T.; Homer, N.; Sedova, M.; Miao, X.; Reed, B.; Sabina, J.; Feierstein, E.; Schorn, M.; Alanjary, M.; Dimalanta, E.; Dressman, D.; Kasinskas, R.; Sokolsky, T.; Fidanza, J. A.; Namsaraev, E.; McKernan, K. J.; Williams, A.; Roth, G. T.; Bustillo, J. An Integrated Semiconductor Device Enabling Non-optical Genome Sequencing. *Nature* **2011**, *475*, 348−352.

(12) Fromherz, P.; Offenhäusser, A.; Vetter, T.; Weis, J. A Neuron-Silicon Junction: a Retzius Cell of the Leech on an Insulated-Gate Field-Effect Transistor. *Science* **1991**, *252*, 1290−1293.

(13) Offenhäusser, A.; Knoll, W. Cell-Transistor Hybrid Systems and Their Potential Applications. *Trends Biotechnol.* **2001**, *19*, 62−66.

(14) Sakata, T.; Saito, A.; Mizuno, J.; Sugimoto, H.; Noguchi, K.; Kikuchi, E.; Inui, H. Single Embryo-Coupled Gate Field Effect Transistor for Elective Single Embryo Transfer. *Anal. Chem.* **2013**, *85*, 6633−6638.

(15) Satake, H.; Saito, A.; Sakata, T. Elucidation of Interfacial pH Behaviour at Cell/Substrate Nanogap for *in situ* Monitoring of Cellular Respiration. *Nanoscale* **2018**, *10*, 10130−10136.

(16) Chen, R. J.; Bangsaruntip, S.; Drouvalakis, K. A.; Kam, N. W. S.; Shim, M.; Li, Y. M.; Kim, W.; Utz, P. J.; Dai, H. J. Noncovalent Functionalization of Carbon Nanotubes for Highly Specific Electronic Biosensors. *Proc. Natl. Acad. Sci. U. S. A.* **2003**, *100*, 4984−4989.

(17) Patolsky, F.; Timko, B. P.; Yu, G.; Fang, Y.; Greytak, A. B.; Zheng, G.; Lieber, C. M. Detection, Stimulation, and Inhibition of Neuronal Signals with High-Density Nanowire Transistor Arrays. *Science* **2006**, *313*, 1100−1104.

(18) Nebel, C. E.; Rezek, B.; Shin, D.; Uetsuka, H.; Yang, N. Diamond for Bio-Sensor Applications. *J. Phys. D: Appl. Phys.* **2007**, *40*, 6443.

(19) Ohno, Y.; Maehashi, K.; Yamashiro, Y.; Matsumoto, K. Electrolyte-Gated Graphene Field-Effect Transistors for Detecting pH and Protein Adsorption. *Nano Lett.* **2009**, *9*, 3318−3322.

(20) Sarkar, D.; Liu, W.; Xie, X.; Anselmo, A. C.; Mitragotri, S.; Banerjee, K. MoS_2 Field-Effect Transistor for Nextgeneration Label-Free Biosensors. *ACS Nano* **2014**, *8*, 3992−4003.

(21) Zhang, Y.; Li, H.; Wang, H.; Xie, H.; Liu, R.; Zhang, S.-L.; Qiu, Z.-J. Thickness Considerations of Two-Dimensional Layered Semiconductors for Transistor Applications. *Sci. Rep.* **2016**, *6*, 295615.

(22) Sucharitakul, S.; Rajesh Kumar, U.; Sankar, R.; Chou, F.-C.; Chen, Y.-T.; Wang, C.; He, C.; He, R.; Gao, X. P. A. Screening Limited Switching Performance of Multilayer 2D Semiconductor FETs: the Case for SnS. *Nanoscale* **2016**, *8*, 19050−19057.

(23) Fang, N.; Nagashio, K. Accumulation-Mode Two-Dimensional Field-Effect Transistor: Operation Mechanism and Thickness Scaling Rule. *ACS Appl. Mater. Interfaces* **2018**, *10*, 32355−32364.

(24) Li, S.-L.; Wakabayashi, K.; Xu, Y.; Nakaharai, S.; Komatsu, K.; Li, W.-W.; Lin, Y.-F.; Aparecido-Ferreira, A.; Tsukagoshi, K. Thickness-Dependent Interfacial Coulomb Scattering in Atomically Thin Field-Effect Transistors. *Nano Lett.* **2013**, *13*, 3546−3552.

(25) Yu, Z.; Ong, Z.-Y.; Li, S.; Xu, J.-B.; Zhang, G.; Zhang, Y.-W.; Shi, Y.; Wang, X. Analyzing the Carrier Mobility in Transition-Metal Dichalcogenide MoS_2 Field-Effect Transistors. *Adv. Funct. Mater.* **2017**, *27*, 1604093.

(26) Yu, Z.; Pan, Y.; Shen, Y.; Wang, Z.; Ong, Z.-Y.; Xu, T.; Xin, R.; Pan, L.; Wang, B.; Sun, L.; Wang, J.; Zhang, G.; Zhang, Y. W.; Shi, Y.; Wang, X. Towards Intrinsic Charge Transport in Monolayer Molybdenum Disulfide by Defect and Interface Engineering. *Nat. Commun.* **2014**, *5*, 5290.

(27) Li, S.; Tian, M.; Gao, Q.; Wang, M.; Li, T.; Hu, Q.; Li, X.; Wu, Y. Nanometre-Thin Indium Tin Oxide for Advanced High-Performance Electronics. *Nat. Mater.* **2019**, *18*, 1091−1097.

(28) Haga, K.; Kamiya, Y.; Tokumitsu, E. Direct Imprinting of Indium−Tin-Oxide Precursor Gel and Simultaneous Formation of Channel and Source/Drain in Thin-Film Transistor. *Jpn. J. Appl. Phys.* **2018**, *57*, No. 02CB14.

(29) Guo, D.; Zhuo, M.; Zhang, X.; Xu, C.; Jiang, J.; Gao, F.; Wan, Q.; Li, Q.; Wang, T. Indium-Tin-Oxide Thin Film Transistor Biosensors for Label-Free Detection of Avian Influenza Virus H5N1. *Anal. Chim. Acta* **2013**, *773*, 83−88.
(30) De Wit, J. H. W.; Van Unen, G.; Lahey, M. Electron Concentration and Mobility in In_2O_3. *J. Phys. Chem. Solids* **1977**, *38*, 819−824.
(31) Das, S. Two Dimensional Electrostrictive Field Effect Transistor (2D-EFET): A sub-60mV/decade Steep Slope Device with High ON current. *Sci. Rep.* **2016**, *6*, 34811.
(32) Vu, Q. A.; Fan, S.; Lee, S. H.; Joo, M.-K.; Yu, W. J.; Lee, Y. H. Near-Zero Hysteresis and Near-Ideal Subthreshold Swing in h-BN Encapsulated Single-Layer MoS Field-Effect Transistors. *2D Mater.* **2018**, *5*, No. 031001.
(33) Kobayashi, M. A Perspective on Steep-Subthreshold-Slope Negative-Capacitance Field-Effect Transistor. *Appl. Phys. Express* **2018**, *11*, 110101.
(34) Sze, S. M.; Kwok, K. *Ng Physics of Semiconductor Devices*; Wiley: New York, 3rd ed. 2007.
(35) Liu, N.; Chen, R.; Wan, Q. Recent Advances in Electric-Double-Layer Transistors for Bio-Chemical Sensing Applications. *Sensors* **2019**, *19*, 3425.
(36) Goebbert, C.; Nonninger, R.; Aegerter, M. A.; Schmidt, H. Wet Chemical Deposition of ATO and ITO Coatings Using Crystalline Nanoparticles Redispersable in Solutions. *Thin Solid Films* **1999**, *351*, 79−84.
(37) Shirahata, N.; Sakka, Y.; Uchikoshi, T.; Hozumi, A. Area-Selective Assembly of High Crystalline Tin-Doped−Indium−Oxide Particles onto Monolayer Template. *J. Vac. Sci. Technol., A* **2005**, *23*, 1146−1151.
(38) Manjakkal, L.; Sakthivel, B.; Gopalakrishnan, N.; Dahiya, R. Printed Flexible Electrochemical pH Sensors Based on CuO Nanorods. *Sens. Actuators, B* **2018**, *263*, 50−58.
(39) Salahuddin, S.; Datta, S. Can the Subthreshold Swing in a Classical FET be Lowered below 60 mV/decade? *IEEE Int. Electron Devices Meet.* **2008**, 1−4.
(40) Nishino, R.; Kozuka, Y.; Kagawa, F.; Uchida, M.; Kawasaki, M. Ferroelectric Field Control of Charge Density in Oxide Films with Polarization Reversal by Electric Double Layer. *Appl. Phys. Lett.* **2018**, *113*, 143501.
(41) Gao, X. P. A.; Zheng, G.; Lieber, C. M. Subthreshold Regime has the Optimal Sensitivity for Nanowire FET Biosensors. *Nano Lett.* **2010**, *10*, 547−552.
(42) Chen, Z.; Yang, K.; Wang, J. Preparation of Indium Tin Oxide Films by Vacuum Evaporation. *Thin Solid Films* **1988**, *162*, 305−313.
(43) Zhang, X.; Jia, F.; Yang, B.; Song, S. Oxidation of Molybdenum Disulfide Sheet in Water under in Situ Atomic Force Microscopy Observation. *J. Phys. Chem. C* **2017**, *121*, 9938−9943.
(44) Artel, V.; Guo, Q.; Cohen, H.; Gasper, R.; Ramasubramaniam, A.; Xia, F.; Naveh, D. Protective Molecular Passivation of Black Phosphorus. *npj 2D Mater. Appl.* **2017**, *1*, 6.
(45) Chen, X.; Shinde, S. M.; Dhakal, K. P.; Lee, S. W.; Kim, H.; Lee, Z.; Ahn, J.-H. Degradation Behaviors and Mechanisms of MoS_2 Crystals Relevant to Bioabsorbable Electronics. *NPG Asia Mater.* **2018**, *10*, 810−820.
(46) Sakata, T.; Nishimura, K.; Miyazawa, Y.; Saito, A.; Abe, H.; Kajisa, T. Ion Sensitive Transparent-Gate Transistor for Visible Cell Sensing. *Anal. Chem.* **2017**, *89*, 3901−3908.
(47) Hattori, M.; Suga, K.; Fujihira, M. Stability of Chemically Modified Indium−Tin−Oxide Surfaces against Water. *Chem. Lett.* **2009**, *38*, 266−267.
(48) Sakata, T.; Kamahori, M.; Miyahara, Y. DNA Analysis Chip Based on Field Effect Transistors. *Jpn. J. Appl. Phys.* **2005**, *44*, 2854−2859.
(49) Satake, H.; Sakata, T. Estimation of Extracellular Matrix Production Using Cultured-Chondrocyte-Based Gate Ion-Sensitive Field-Effect Transistor. *Anal. Chem.* **2019**, *91*, 16017−16022.

https://doi.org/10.1021/acsami.1c05830
ACS Appl. Mater. Interfaces XXXX, XXX, XXX−XXX